Appl Magn Reson (2014) 45:681–692
DOI 10.1007/s00723-014-0546-2

Applied
Magnetic Resonance

A Multifrequency (X-, Q-, and W-band) EPR and DFT Study of a Photopolymerizable Dental Resin

Adriana da Silva Fontes · Bruno Luiz Santana Vicentin · Daniel Farinha Valezi · Marcello Ferreira da Costa · Walter Sano · Eduardo Di Mauro

Received: 21 February 2014 / Revised: 12 June 2014 / Published online: 27 June 2014

Abstract The free radicals generated during the polymerization process of Z100 (3 M ESPE) dental resin were examined by electron paramagnetic resonance (EPR) in X-, Q- and W-bands. Experimental generation and spectra simulations were associated with density functional theory (DFT) calculations to determine the molecular structure and explain the EPR spectrum formation. It was assumed that the EPR spectrum was formed by the sum of two different types of radicals: "propagating" and allylic. The spectra simulations and DFT calculations showed good agreement, indicating that the proposed model fully explained the nine lines of the EPR spectrum in X-band and showed that the spectrum formation is the sum of "9 + 5" lines, rather than the "5 + 4" lines predicted early. Simulations in Q- and W-bands showed very close correlation and were essential to support the proposed model.

1 Introduction

Photopolymerizable resins are the best substitutes for restoring the lost part of a tooth, both esthetically and practically, because a substitute with similar properties to the human tooth still does not exist. However, these resins do not polymerize completely and this causes problems that can compromise the restoration. Numerous factors affect polymerization, including chemical composition, polymerization conditions, light intensity and distance from the device to the resin, which can compromise the

A. da Silva Fontes
Department of Physics, Federal University of Technology of Paraná, Campo Mourão 87301-899, Brazil

B. L. S. Vicentin (✉) · D. F. Valezi · M. F. da Costa · E. Di Mauro
Department of Physics, State University of Londrina, Londrina 86057-970, Brazil
e-mail: bruno.vicentin@uel.br

W. Sano
Institute of Physics, University of São Paulo, São Paulo 05508-090, Brazil

restoration and cause problems, such as contraction, poor mechanical strength, color change and infiltration. In order to avoid these problems and improve the mechanical properties of the restoration, a clearer understanding of the polymerization process is important. This process continues even when there is no incident radiation and the free radicals generated during irradiation are responsible for its continuation [1].

For more than 40 years, EPR spectroscopy has been used to detect, characterize and monitor the evolution of free radical concentration in dental resins. This spectroscopic technique has been used to study the behavior of the methacrylate radical generated during the photopolymerization of dental restoration resins in numerous situations, including: irradiation at different wave lengths [2], required polymerization time as a function of resin composition [3] or sample thickness [4], resin hardness as a function of the relative number of radicals [5, 6], conversion degree [7], analysis of polymerization initiator agents [8, 9], real-time study of polymerization kinetics [7, 10, 11], variations in the monomer matrix and influence on the chemical reaction [12, 13], the effect of the saturation time [12, 13], evaluation of the behavior of free radicals versus mechanical properties [14], the relation between the free radicals generated and polymerization depth in resin with different colors [15], and translucence [16]. Some research has been conducted to elucidate the well-known, though not fully interpreted, nine-line EPR spectrum obtained in X-band for the radicals of methacrylate monomers. Some authors have attributed this spectrum to only one radical specimen [12, 13, 17–20]. It is currently accepted that this spectrum is due to at least two different free radical types, which are assumed to occur simultaneously in the samples under study [21–23]. Some authors [3, 8, 9, 21] assumed that the EPR spectrum is formed by the sum "5 + 4" lines; however, the intensities of the lines obtained using this model are different from those in the dental resin spectrum. Others have assumed that the spectrum is generated from two methacrylate radicals in the solid state (Fig. 1), the "propagating" radical (RI) and the allylic radical (RIII). In addition, the methacrylate radical (RII) is probably not observed in the EPR spectrum because it reacts rapidly or the quantity generated is too small to detect, such that the resulting EPR spectrum is formed by the superposition of "9 + 5" lines [22]. This was the model adopted in this paper.

This study was developed due to the lack of consensus regarding the interpretation of dental resin EPR spectra in X-band. The research yielded new contributions concerning the nature of the EPR spectra, obtained in X-, Q- and W-bands, with their respective simulations assuming the involvement of the free radicals described above. The hyperfine interactions were calculated using DFT methodology (UB3LYP) and 6–31 + g(3df) basis sets [24] and the values obtained showed good agreement with the experimental results.

2 Experimental

2.1 Materials

Samples of the commercial resin Z100 (3 M ESPE, Campinas, SP, Brazil), in A2 color indicated for dental enamel, were used in the EPR experiments. It is composed

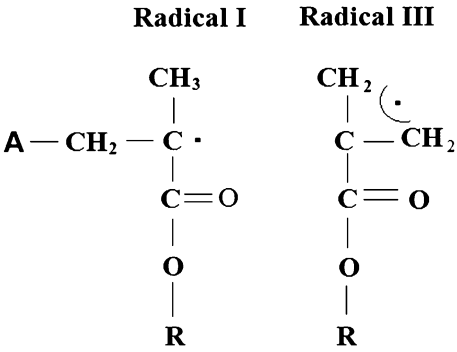

Fig. 1 Free radicals generated during the photopolymerization of dental resin Z100 (3 M ESPE) that are responsible for the EPR spectrum formation, where A is the amine monomer and R is dimethacrylate monomer mixture of Bis-GMA and TEGDMA

essentially of a dimethacrylate monomer mixture of Bis-GMA and TEGDMA, initiator agents (Camphorquinone and Amine) and charge particles of zirconium and silica (ZrO_2/SiO_2) (manufacturer's specifications). The light source used for photopolymerization was a LED (Ultra Blue, Dabi Atlante, Ribeirão Preto, SP, Brazil) with an intensity 492 mW/cm^2 for 40 s.

2.2 Electron Paramagnetic Resonance Spectroscopy and Spectrum Simulation

The EPR spectra in X-band ($\sim$9 GHz) were obtained on a JEOL (JES-PE-3X) spectrometer at room temperature, and the microwave power (1 mW), modulation amplitude (0.40 mT) and modulation frequency (100 kHz) were set to avoid signal saturation and were maintained constant. A JEOL standard sample MgO:Mn^{2+} was used as intensity standard and g marker. The samples were placed in a 2 $\times$ 2 mm silicon mold and investigated immediately following 40 s of irradiation [16]. The EPR spectra in Q-band were measured on a VARIAN (E-109) spectrometer, with rectangular cavity, microwave power 0.5 mW and modulation amplitude 0.40 mT. A MgO:Cr^{3+} was used as intensity standard and g marker, where $g = 1.9797$. The samples were placed in a 1 $\times$ 1 mm silicon mold and irradiated for 40 s. The EPR spectra in W-band were obtained in a Bruker (Elexsys E 680) spectrometer with TerraFlex probe, with samples' dimensions of less than 1 mm. The data treatment was performed with the Origin (OriginLab) software, and simulations were achieved using the WinEPR (Bruker) software.

2.3 DFT Calculations of Molecular Structure

The calculations were carried out using the program package NWChem [24]. The geometry optimizations were performed at the UB3LYP/6–31 + g(3df) level of the theory, and they were carried out with no constraints or restraints, and all energies (in 10^{-6} kcal mol^{-1}) are given as obtained, with zero-point correction. The geometries were checked by frequency calculations to confirm that they were minima (zero imaginary frequencies) or transition states (one imaginary frequency).

3 Results and Discussion

3.1 X-Band EPR Spectrum Simulation

The EPR spectrum in X-band of the Z100 (3 M ESPE) composite resin is identical to that observed for methacrylate systems, and it is thus attributed to the sum of two different radical types, the "propagating" radical and the allylic radical [22]. Furthermore, these radicals are not dependent on the amount or type of additive substances used for color control and translucence, and also do not depend on inorganic fillers or the light source [14].

Changes in the polymerization environment have a significant effect on EPR spectra, which are observed as a function of the extent of polymerization. Initially, a 13-line spectrum was observed, corresponding to free radicals in a mobile liquid-like environment. However, as polymerization progressed, this changed to a 9-line EPR spectrum, which has been attributed to the same radicals within a network presenting restricted mobility [7, 25]. The free radicals produce an EPR signal with hyperfine splitting, and the resulting spectrum shows an intense signal that remains detectable up to 3 months after the polymerization process began, depending on the storage environment [26] and relative concentration generated [14].

The EPR spectrum was simulated based on the model proposed by Trufier-Boutry et al. [22], as shown in Fig. 2. Radical I is the "propagating" methacrylate radical (CH_2–C.–CH_3) that shows a weak nine-line signal; while the other simulated radical, RIII (CH_2–C.–CH_2), has a strong five-line signal arising from a stable radical, called an allylic radical (Fig. 2b) [22]. The EPR spectrum of polymethacrylate radicals consists of the superposition of 9-line (RI) and 5-line (RIII) sets resulting in a "9-line spectrum" with peaks of alternating intensities, because the hyperfine interaction of the 5-line set is about twofold greater than that of the 9-line set and the first line of both sets are virtually coincident. Thus, the proposed model is a "9 + 5 line spectrum", and not a "5 + 4 line spectrum", since the mathematical simulation of the spectrum with this model is very close to the EPR spectrum Fig. 3. Regarding the spectrum simulation, Lorentzian and Gaussian shapes were both considered, with different proportions, because these two line shapes are commonly observed in EPR [27].

The area of the spectrum integral is a reliable measurement of the spin density, and hence of the concentration for each radical type. It should be emphasized that the intensity of the central peak is the sum of the central peak intensities (more intense line of the spectrum) of both species. Nevertheless, the intensity of the "propagating" species (fourth peak) was low compared with the intensity of the allylic species (central peak), such that its contribution was not expected to be more than 10 % of the measured intensity [28].

The spin Hamiltonian for radicals I and III can be represented as $H_I = g\beta HS + [AIS + BIS + B'IS]$ for radical I, and $H_{III} = g\beta HS + [AIS + BIS]$ for radical III, where $g\beta HS$ is the Zeeman effect, AIS, BIS and B'IS are the hyperfine interactions of first and second orders, respectively. The hyperfine structure with nine lines was interpreted and simulated in terms of an unpaired

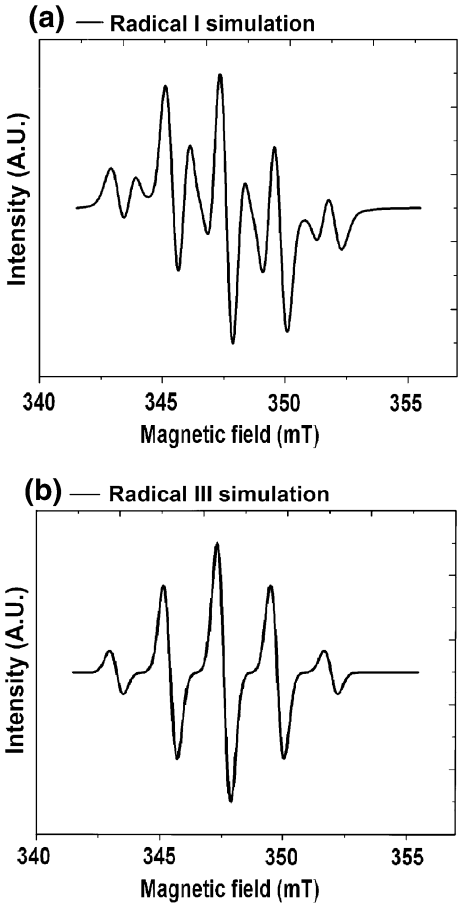

Fig. 2 Radical I (**a**) and radical III (**b**) EPR spectra simulations of the composite resin in X-band

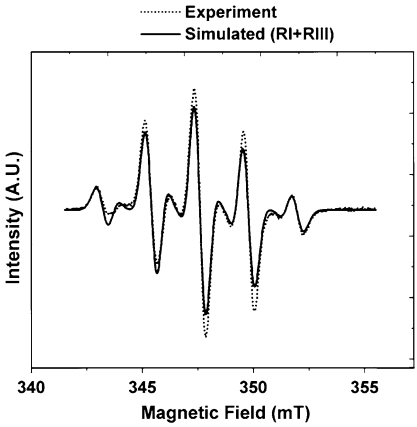

Fig. 3 Superposition of simulated "RI + RIII" and experimental spectra

electron interaction, with three equivalent protons of the CH_3 group and two non-equivalent protons of the CH_2 group for radical I, and the interaction of radical III with two CH_2 groups, the radical generated during hydrogen abstraction of the monomer by an amine radical [16]. The parameters obtained for the simulation in X-band for radical I, with $S = 1/2$ and $I = 1/2$, were: $g = 2.0051$; $A/g\beta = 2.17$ mT for three equivalent ½ spin protons belonging to the CH_3 group; $B/g\beta = 1.40$ mT for a non-equivalent proton belonging to the CH_2 group and $B'/g\beta = 0.85$ mT for a second non-equivalent proton belonging to the CH_2 group. For radical III, the parameters used were: $g = 2.0051$; $A/g\beta = 2.17$ mT for two equivalent ½ spin protons belonging to the CH_2 group; and $B/g\beta = 2.17$ mT for two equivalent ½ spin protons belonging to the second CH_2 group [16].

Other EPR spectra obtained in X-band are shown in Fig. 4. The spectra in Fig. 4a were obtained every 2 s for the resin irradiated in the spectrometer cavity during 200 s. An increase in radical concentration was verified as irradiation time increased. Our observations confirmed that the EPR spectra presented the same characteristics from the beginning to the end of the photoactivation process, indicating the same species of free radicals in the sample.

We plotted the relative intensity for the two radicals formed during the irradiation in Fig. 4b. It was evident that the quantity of the allylic radical generated was greater than that of the "propagating" radical. The relative intensity of generated radicals was obtained by measuring the area of the fourth and fifth peaks of the integrated "9-line spectrum" for allylic and "propagating" radicals, respectively.

3.2 Q-Band EPR Spectrum Simulation

In order to obtain additional information concerning the radicals that participate in the polymerization process, measurements were performed in other EPR bands, aimed at improving the spectrum resolution due to the use of higher frequencies. The same model was tested using the Q- and W-bands, due to their sensitivity, to detect other radical species; non-detection can occur when the radical is produced in very small amounts or in the case of species possessing very similar g factors. Since no changes in the spectrum formation were verified, the hypothesis of two radicals was considered valid.

The EPR spectrum in Q-band ($\sim$34 GHz) and its computational simulation are presented in Fig. 5. Figure 5a shows the simulation of radical I, Fig. 5b shows the simulation of radical III and Fig. 5c shows what happens when the simulations of radicals I and III are superposed and compared with the EPR spectrum. Fewer lines are observed in Q- (7 lines) than in X-band (9 lines). Some of these lines are superposed, hindering the identification of the same. A slightly different result for the hyperfine interaction in relation to the X-band spectrum was obtained in Q-band, by means of the simulation. For the A_{zz} direction of the CH_3 group (from 2.3 to 2.50 mT), the g_z value for Radical I was also different.

The spin Hamiltonian for radicals I and III can be represented as $H_I = g\beta HS + [AIS + BIS + B'IS]$ for radical I, and $H_{III} = g\beta HS + [AIS + BIS]$ for radical III, where $g\beta HS$ is the Zeeman effect, AIS, BIS and B′IS are the hyperfine interactions of first and second orders, respectively. The parameters for

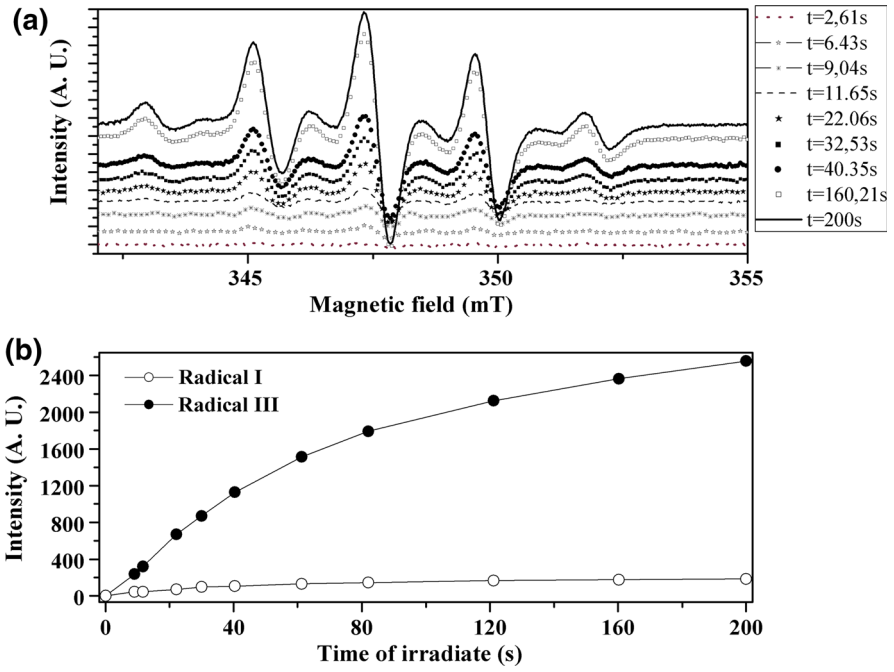

Fig. 4 **a** EPR spectra obtained during irradiation by a LED source in the spectrometer cavity. **b** The increase in radical concentration vs. irradiation time

the simulation with ½ spin for radical I were: $A_{CH3x}/g\beta = 2.32$ mT, $A_{CH3y}/g\beta = 2.32$ mT, $A_{CH3z}/g\beta = 2.33$ mT for three protons of the CH_3 group; $B_{CH2x}/g\beta = 1.30$ mT, $B_{CH2y}/g\beta = 2.00$ mT, $B_{CH2z}/g\beta = 1.60$ mT for one proton of the CH_2 group; $B'_{1CH2x}/g\beta = 0.95$ mT, $B'_{1CH2y}/g\beta = 0.75$ and $B'_{1CH2z}/g\beta = 0.93$ mT for one second proton of the CH_2 group; $g_x = 2.0015$, $g_y = 2.0023$, $g_z = 2.0023$, L/G = 0.5, $l_x = l_y = 0.59$ mT and $l_z = 0.60$ mT. For radical III, $A_{CH2xyz}/g\beta = 2.34$ mT and $B_{CH2xyz}/g\beta = 2.34$ mT are two CH_2 groups with four equivalent protons, $g_{xyz} = 2.0020$, $l_x = l_y = 0.55$ mT and $l_z = 0.61$ mT.

3.3 W-Band EPR Spectrum Simulation

The W-band (~94 GHz) EPR spectrum is obtained and its respective simulation and corresponding superposition of radicals I and III are presented in Fig. 6. Analysis of the figures revealed that improvement in the EPR spectrum resolution is observed when a higher microwave frequency is used, due to the fact that the free radicals present in the resin are submitted to a more intense magnetic field, which permits the observation of a larger portion of the resonance lines of each radical. The majority of the transitions observed in W-band occur in the region of superposed energy levels, hindering clearer identification of the same in X- and Q-bands. The advantage of measuring at higher frequencies is the improved resolution, which should assist in differentiating the paramagnetic species. The

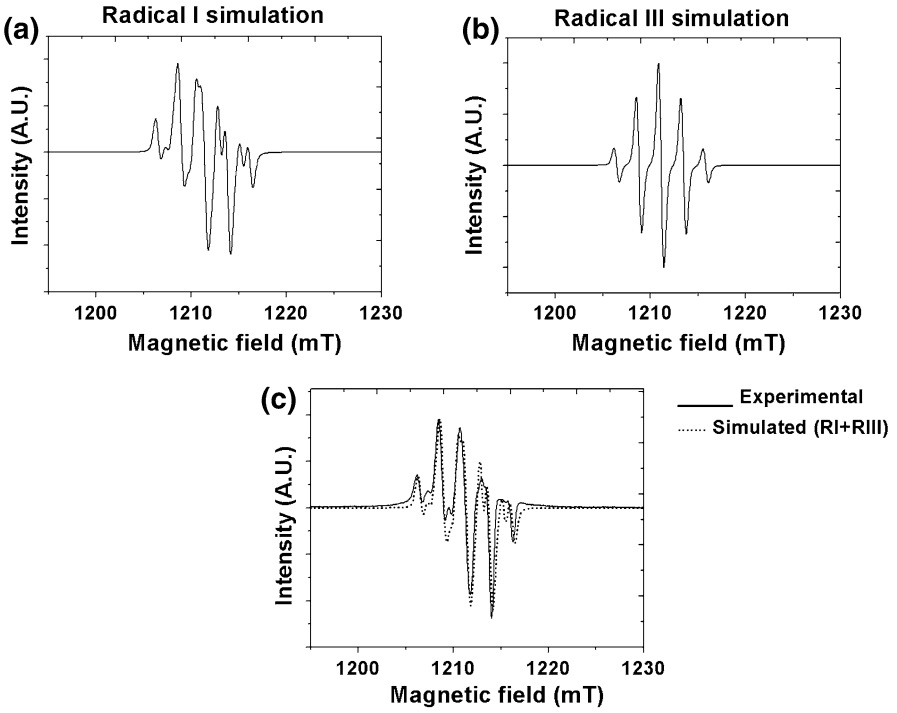

Fig. 5 Radical I (**a**) and radical III (**b**), EPR spectra simulations of the composite resin in Q-band. (**c**) Superposition of the simulated "RI + RIII" and experimental spectra

simulations were performed considering the EPR spectrum formed by the same radical species presented in Fig. 2, i.e., Radical I, represented by the spectrum in Fig. 6a, and Radical III, represented by the spectrum in Fig. 6b. Figure 6c presents the superposition of the spectra and its mathematical simulation.

The spin Hamiltonian for radicals I and III can be represented as $H_I = g\beta HS + [AIS + BIS + B'IS]$ for radical I, and $H_{III} = g\beta HS + [AIS + BIS]$ for radical III, where $g\beta HS$ is the Zeeman effect, AIS, BIS and B′IS are the hyperfine interactions of first and second orders, respectively. The parameters for the simulation with ½ spin for radical I were: $A_{CH3x}/g\beta = 2.46$ mT, $A_{CH3y}/g\beta = 2.48$ mT, $A_{CH3z}/g\beta = 2.50$ mT for three protons of the CH_3 group; $B_{CH2x}/g\beta = 1.30$ mT, $B_{CH2y}/g\beta = 1.40$ mT, $B_{CH2z}/g\beta = 1.45$ mT for one proton of the CH_2 group; $B'_{1CH2x}/g\beta = 0.95$ mT, $B'_{1CH2y}/g\beta = 0.75$ and $B'_{1CH2z}/g\beta = 0.90$ mT for one second proton of the CH_2 group; $g_x = 2.00069$, $g_y = 2.0028$, $g_z = 2.0023$, L/G = 0.5, $l_x = l_y = 0.59$ mT and $l_z = 0.65$ mT. For radical III, $A_{CH2xyz}/g\beta = 2.34$ mT and $B_{CH2xyz}/g\beta = 2.34$ mT are two CH_2 groups with four equivalent protons, $g_{xyz} = 2.0020$, $l_x = l_y = 0.55$ mT and $l_z = 0.61$ mT.

Some lines not observed in X- and Q-bands were observed in the measurements performed in W-band. It has been postulated that methacrylate radicals exhibit an EPR spectrum in X-band of 13 lines in an atmosphere similar to a liquid state and a

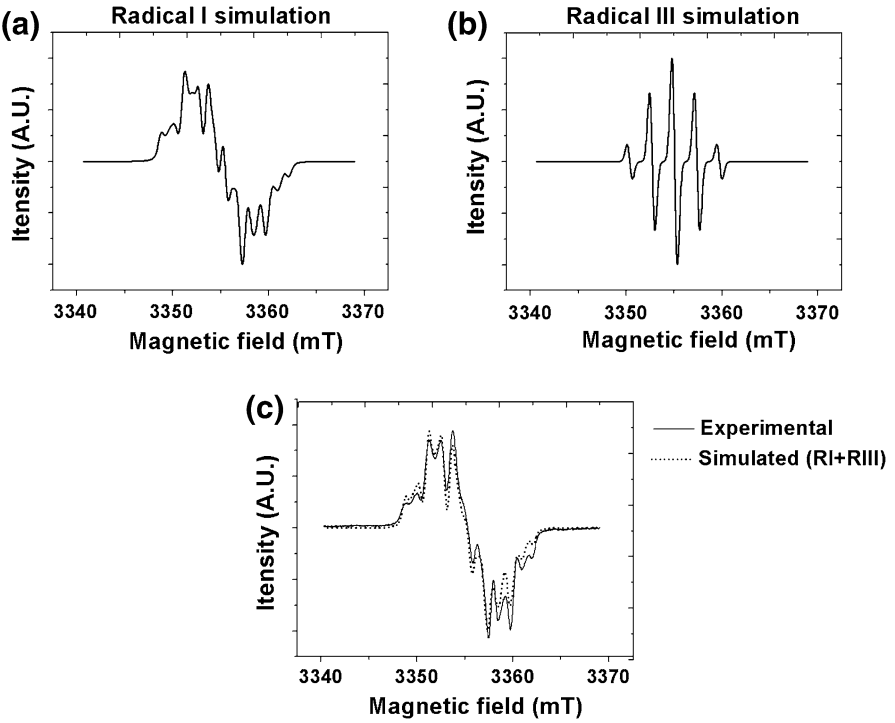

Fig. 6 EPR spectrum formation for the dental resin obtained in W-band. Radical I (**a**) and radical III (**b**), and the superposition of the experimental spectrum and the sum of the simulated spectra of radicals I and III (**c**)

spectrum of 9 lines in a solid-like system [7], but such EPR spectra were obtained at low temperature or using a different spectroscopy technique (ENDOR), thus facilitating the visualization of transitions not previously observed in common EPR in X-band. One explanation for the EPR spectrum with 13-lines observed here is the greater resolution of the spectrometer due to the higher frequency used, and the consequent improvement in differentiating between radicals I and III.

In relation to the some little differences between experiments and simulations, it is important to remember that we simulate considering the macromolecular system with the unpaired electron interacting only with the closer vicinity, and the Hamiltonian is an approximation for this system in vacuum or water environment. The polymerization of the sample itself can also influence in the result. Considering the number of peaks, line shape and other parameters, the simulations are in good agreement with experiment.

3.4 DFT Calculations of Molecular Structure

The DFT methodology was used, specifically the UB3LYP functional, which is a hybrid method that combines the Becke three-parameter exchange functional with

the nonlocal correlation functional of Lee et al. [24]. Because of the size of the system analyzed, the computations were performed using basis sets of contracted Gaussian functions, namely, 6–31 + g(3df). The 6–31 + g(3df) is a relatively large basis set including an f-polarization function. The larger 6–31 + g(3df) was used to optimize the geometry of the most stable conformation of the radical model, and was used again later to obtain the hyperfine tensors.

This computational protocol UB3LYP/6–31 + g(3df) (Fig. 7) is very adequate for performing calculations of coupling constants for medium size radicals, because it provides accurate values of this property. For calculation purposes, the 3 × 3 hyperfine interaction tensor can be separated into its isotropic (spherically symmetric) and anisotropic (dipolar) components. For first-order isotropic hyperfine interactions, $A_{\mathrm{iso}}(N)$ are related to the spin densities $\rho^{\mathrm{s}}(r_N)$ at the corresponding nuclei by:

$$A_{\mathrm{iso}}(N) = (8\pi/3) g_e g_N \beta_N \beta_e \rho^S(r_N), \tag{1}$$

where β_e and β_N are the electron and nuclear magneton, respectively; g_e and g_N are the corresponding magnetogyric ratios, $\rho(r_{\mathrm{N}})$ is the spin density on the nucleus N, which is just $\rho(\gamma_N) = |\varphi(r)|^2$, where $\varphi(r)$ is the molecular orbital containing the unpaired electron. In our particular case, the spin density is expressed as:

$$\rho_T(\gamma_N) = \sum_{i=1}^{N_\alpha} \left|\phi_i^\alpha(\vec{r})\right|^2 - \sum_{i=1}^{N_\beta} \left|\phi_i^\beta(\vec{r})\right|^2. \tag{2}$$

The isotropic component can be obtained from the Fermi contact analysis given by most calculations of modern electronic structure. The anisotropic components can be obtained from the spin only electric field gradient tensors. The simulation is conducted in gaseous phase, and the contribution to the anisotropic part is null. Experimentally, in the solid state, the total tensor is observed, i.e., isotropic plus anisotropic components [29].

According to our calculations, the hyperfine constants of the β and β′ protons were 1.48 and 0.72 mT, respectively, and the mean value calculated (2.08 mT) corresponds to protons of the methyl group. These computed hyperfine coupling constants were in good agreement with the data obtained from the experimental spectra (1.40, 0.85 and 2.17 mT, respectively).

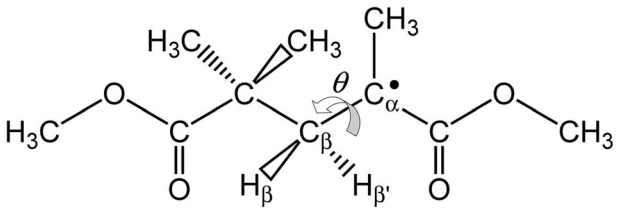

Fig. 7 UB3LYP/6–31 + g(3df) model used for DFT calculations

4 Conclusions

The EPR spectrum obtained in our analysis of the composite resin used for dental restoration is characteristic of methacrylate resins and throughout the analysis performed in X-, Q- and W-bands, it was interpreted as two methacrylate free radical species: (–CH_2–C.–CH_3–) and (–CH_2–C.–CH_2–), denominated Radical I ("propagating" radical) and Radical III (allylic radical), respectively. These two species are responsible for the continuity of the resin polymerization process following irradiation. No new information concerning the nature of the radicals was observed using EPR in Q- and W-bands, but these measurements and their simulations confirmed that the proposed model, involving the two radicals cited above, is entirely sufficient to explain the EPR spectra of the dental resin. The hypothesis of the existence of other free radicals in the formation of the dental resin spectrum can be abandoned, since the simulation of other free radicals (Ceto, Amino, and Radical II) does not fit the EPR spectrum.

Acknowledgments We thank the EPR Division of Bruker-BioSpin GmbH (Germany) for recording the spectra in W-band, Dr. Otaciro Rangel Nascimento and José Fernando Lima (of the "Sergio Mascarenhas" Molecular Biophysics Group, USP, São Carlos, Brazil) for EPR spectra in Q-band, and Dr. Julian G. Leprince (Université Catholique de Louvain, Belgium), for his valuable insights/assistance in discussions concerning this research.

References

1. H.R. Rawke, J. Escjuivel-Upshaw in *Phillips Materiais Dentários*, 10th edn., ed. by K.J. Anusavice, S.A. Guanabara Koogan (Rio de Janeiro, 1998), Chapter 15, p. 386
2. A.T. Bullock, L.H. Sutcliffe, Trans. Faraday Soc. **8**, 625–633 (1964)
3. M.F. Ottaviani, A. Fiorini, P.N. Mason, C. Corvaja, Dent. Mater. **8**, 118–124 (1992)
4. D. Cevc Sustercic, N.P. Funduk, M.M. Pintar, J. Mater. Sci. Mater. Med. **8**, 507–510 (1997)
5. M.A. Menezes, A. Muench, Rev. Odontol. Univ. São Paulo **12**, 281–285 (1998)
6. W. Sano, C.B.M. Mello, Rev. Bras. Eng. Biomed. **15**, 17–20 (1999)
7. L.G. Lovell, K.A. Berchtold, J.E. Elliott, H. Lu, C.N. Bowman, Polym. Adv. Technol. **12**, 335–345 (2001)
8. L. Lapcik Jr, J. Jancar, A. Stasko, P. Saha, J. Mater. Sci. Mater. Med. **9**, 257–262 (1998)
9. W. Teshima, Y. Nomura, N. Tanaka, H. Urabe, M. Okazaki, Y. Nahara, Biomaterials **24**, 2097–2103 (2003)
10. W. Sano, C.B.M. Mello, SBPN Scientif. J. **5**(1), 368–369 (2001)
11. J. Leprince, G. Lamblin, D. Truffier-Boutry, S. Demoustier-Champagne, J. Devaux, M. Mestdagh, G. Leloup, Acta Biomate **5**, 2518–2524 (2009)
12. D.C. Doetschman, R.C. Mehlenbacher, D. Cywar, Macromolecules **29**(5), 1807–1816 (1996)
13. S.G. Pereira, J.P. Telo, T.G. Nunes, J. Mater. Sci. Mater. Med. **19**(9), 3135–3144 (2008)
14. A.S. Fontes, E. Di Mauro, W. Sano, N.C.S. Lima, L.H. Dall'Antonia, Polímeros **19**(4), 285–291 (2009)
15. J. Leprince, P. Leveque, B. Nysten, B. Gallez, J. Devaux, G. Leloup, Dent. Mater. **28**, 512–520 (2012)
16. A.S. Fontes, W. Sano, L.H. Dall'Antonia, E. Di Mauro, Appl. Magn. Reson. **39**(4), 381–390 (2010)
17. H. Fischer, J. Polym. Sci. B Polym. Lett. **2**(5), 529–532 (1964)
18. M. Iwasaki, Y. Sakai, J. Polym. Sci. A1 Polym. Chem. **7**(6), 1537–1547 (1969)
19. M. Langel, S.R.W. Louro, Nucl. Instrum. Methods Phys. Res. B **16**(4–5), 419–423 (1986)
20. L. Hermosilla, C. Sieiro, P. Calle, M. Zerbetto, A. Polimeno, J. Phys. Chem. B **112**, 11202–11208 (2008)
21. A.T. Bullock, L.H. Sutcliffe, Trans. Faraday Soc. **60**, 2112–2124 (1964)

22. D. Truffier-Boutry, X.A. Gallez, S. Demoustier-Champagne, J. Devaux, M. Mestdagh, B. Champagne, G. Leloup, J. Polym. Sci. A Polym. Chem. **41**(11), 1691–1699 (2003)
23. T.F. Scott, W.D. Cook, J.S. Forsythe, C.N. Bowman, K.A. Berchtold, Macromolecules **36**, 6066–6074 (2003)
24. M. Valiev, E.J. Bylaska, N. Govind, K. Kowalski, T.P. Straatsma, H.J.J. van Dam, D. Wang, J. Nieplocha, E. Apra, T.L. Windus, W.A. de Jong, Comput. Phys. Commun. **181**, 147–1489 (2010)
25. K.A. Berchtold, T.W. Randolph, C.N. Bowman, Macromolecules **38**, 6954–6964 (2005)
26. J.G. Leprince, G. Lamblin, J. Devaux, M. Dewaele, M. Mestdagh, W.M. Palin, B. Gallez, G. Leloup, J. Dent. Res. **89**(12), 1494–1498 (2010)
27. J.W. Orton, *Electron Paramagnetic Resonance*, 2nd edn. (ILIFFE Books, London, 1968), p. 24
28. P. Levêque, J. Leprince, S. Bebelman, J. Devaux, G. Leloup, B. Gallez, J. Magn. Reson. **220**, 45–53 (2012)
29. J. Vaara, J. Jokisaari, R.E. Wasylishen, D.L. Bryce, Prog. Nucl. Magn. Reson. Spectrosc. **41**(3–4), 233–304 (2002)